www.sciencemag.org/content/360/6391/915/suppl/DC1

Supplementary Materials for

An ingestible bacterial-electronic system to monitor gastrointestinal health

Mark Mimee*, Phillip Nadeau*, Alison Hayward, Sean Carim, Sarah Flanagan, Logan Jerger, Joy Collins, Shane McDonnell, Richard Swartwout, Robert J. Citorik, Vladimir Bulović, Robert Langer, Giovanni Traverso, Anantha P. Chandrakasan†, Timothy K. Lu†

*These authors contributed equally to this work.
†Corresponding author. Email: timlu@mit.edu (T.K.L.); anantha@mtl.mit.edu (A.P.C.)

Published 25 May 2018, *Science* **360**, 915 (2018)
DOI: 10.1126/science.aas9315

This PDF file includes:

Materials and Methods
Figs. S1 to S14
Table S1
Captions for tables S2 and S3
References

Other Supplementary Materials for this manuscript include the following:
(available at www.sciencemag.org/content/360/6391/915/suppl/DC1)

Tables S2 and S3 (Excel)

Materials and Methods

Bacterial Strains and Culture Conditions

Routine cloning and plasmid propagation was performed in *E. coli* DH5α. Gene circuits were initially prototyped in *E. coli* MG1655 and were transferred into probiotic *E. coli* Nissle 1917 for capsule and *in vivo* experiments. Cells were routinely cultured at 37˚C in Luria-Bertani (LB) media (Difco). Where appropriate, growth media was supplemented with antibiotics at the following concentrations: 30 µg/mL kanamycin, 100 µg/mL carbenicillin, 25 µg/mL chloramphenicol and 100 µg/mL spectinomycin.

Genetic Part and Plasmid Construction

Genetics parts and plasmids used in this study are listed in Table S2 and Table S3 and will be available from Addgene upon publication. All plasmids were constructed by combining PCR fragments generated by Kapa HiFi Polymerase using Gibson Assembly (*31*). Assembly products were transformed into chemically competent *E. coli* DH5α (*32*) and sequences were confirmed using Sanger sequencing. Ribosome binding sites (RBSs) of variable strengths were computationally designed using the Salis lab RBS calculator (*33*, *34*).

Growth and Induction

For genetic circuit characterization, overnight cultures were diluted 1:100 in fresh LB and incubated with shaking at 37˚C for 2 hours. Cultures were removed from the incubator and 200 µL of culture was transferred to a 96-well plate containing various concentrations of inducer. The plate was returned to a shaking incubator at 37˚C. Following 2 hours of incubation, luminescence was read using a BioTek Synergy H1 Hybrid Reader using a 1s integration time and a sensitivity of 135. Luminescence values, measured in relative luminescence units (RLUs), were normalized by the optical density

of the culture measured at 600 nm. Note that the signal-to-noise ratio (SNR) of the thiosulfate and AHL gene circuits is lower compared to the blood sensing construct. The distinct characteristics of the molecular components involved in analyte sensing, such as the diffusivity of inducer into the cell, binding affinities of inducer to transcription factors and of transcription factors to promoter sequences, cooperativity of transcription factors, and promoter strength, yield distinct transfer functions that could affect SNR. Performance could be further improved by alterations in DNA copy number, promoter sequence, or RBS sequence of genetic circuit components to optimize for greater SNR, overall output, or sensitivity.

For *in vitro* kinetic studies, subcultured cells were mixed with inducer in a 96-well plate and immediately placed in the plate reader set at 37˚C without shaking. Luminescence and absorbance was read at 5 minute intervals. For pH sensitivity studies, citrate-buffered LB at various pHs was made by supplementing LB media with appropriate volumes of 0.2M sodium phosphate dibasic (Sigma) and 0.1M citric acid (Sigma) and adjusted to the desired pH with HCl.

A stock solution of hemin (Sigma) was prepared by dissolving hemin powder in 1M NaOH (Sigma) to a concentration of 25 mM, diluting with double distilled water to a final concentration of 500 µM and sterilizing with a 0.2 µm polyethersulfone (PES) filter. Defibrinated horse blood (Hemostat) was used as the source of blood for most experiments. Blood was lysed by first diluting 1:10 in simulated gastric fluid (SGF) (0.2% NaCl, 0.32% pepsin, 84 mM HCl, pH 1.2) before further dilution in culture media. Stock solutions of sodium thiosulfate (Sigma) and 3-O-C_6-HSL (referred to as acyl homoserine lactone (AHL)) (Cayman Chemical) were made in double distilled water.

Indomethacin Mouse Experiments

All mouse experiments were approved by the Committee on Animal Care at the Massachusetts Institute of Technology. Specific-pathogen free (SPF), male C57BL/6J mice (8-10 weeks of age) were purchased from Jackson Labs and were housed and handled under conventional conditions. Mice were acclimated to the animal facility 1 week prior to the commencement of experiments. Animals were randomly allocated to experimental groups. Researchers were not blinded to group assignments. Prior to indomethacin experiments, a pilot experiment was conducted to determine the transit rate of bacteria through the mouse gastrointestinal tract (Figure S6A). Overnight cultures of *E. coli* Nissle were centrifuged at 5000g for 5 minutes and resuspended in an equal volume of 20% sucrose. Animals were inoculated with 200 µL of bacteria culture (approximately $2x10^8$ CFU) by oral gavage. Fecal pellets were collected 2, 4, 6, 8, and 24 hours post-gavage, weighed, and homogenized in 1mL of PBS with a 5 mm stainless steel bead using a TissueLyser II (Qiagen) at 25 Hz for 2 minutes. Samples were centrifuged at 500g for 30 seconds to pellet large fecal debris. Supernatant was serially diluted in sterile PBS and spot plated on MacConkey agar supplemented with kanamycin. Colonies were enumerated following overnight incubation at 37˚C. For luminescence assays, luminescence in fecal homogenate was measured in a Biotek Synergy H1 Hybrid Reader with an integration time of 1 second and a sensitivity of 150. Luminescence values were normalized to stool weight normalized CFU values and reported in RLU/CFU.

For indomethacin experiments, animals were inoculated with blood sensor bacteria and fecal pellets were collected 6 hours later for luminescence analysis and CFU

enumeration. Indomethacin (Sigma) solution was prepared by dissolving the compound in absolute ethanol to a concentration of 20 mg/mL. Immediately prior to mouse gavage, the indomethacin stock solution was diluted to 1.25 mg/mL in PBS and 0.2 mL of dilute indomethacin solution was administered to each animal (10 mg/kg). Preparation of indomethacin solution using this method was essential to ensure reliable and reproducible induction of gastrointestinal bleeding. The following morning, gastrointestinal bleeding was confirmed by performing a guaiac test (Hemoccult, Beckman Coulter) on fecal pellets from each animal. All mice administered indomethacin were guaiac positive, whereas those administered a PBS control were uniformly guaiac negative. Subsequently, mice were again administered blood sensor bacteria and fecal pellets were collected 6 hours later for luminescence analysis and CFU enumeration. Additional variation was observed in the animal model compared to the *in vitro* experiment of Fig 1B and could be explained by variations in volume of the gastrointestinal tract, transit time of both biosensors and blood, and the level of bleeding achieved by indomethacin administration, among other causes.

Preparation of capsules

The electronics in the capsules consisted of four phototransistor detectors (SFH3710, Osram Opto Semiconductors GmbH), a custom bioluminescence detector chip fabricated in a TSMC 65 nm process (*18*), a microcontroller and radio chip (PIC12LF1840T39A, Microchip Technology Inc.), 22 MHz crystal resonator (7M-22.000MEEQ-T, TXC Corporation), 915 MHz chip antenna (0915AT43A0026, Johanson Technology Inc.), two 220 µF ceramic capacitors (CL32A227MQVNNNE, Samsung Electro-Mechanics America, Inc.), and a 5 mAh lithium manganese button-cell battery

(MS621FE-FL11E, Seiko Instruments Inc.). The electronics were soldered onto custom four-layer printed circuit boards (Advanced Circuits Inc.) and two screws were epoxied into mounting holes for later attachment of the plastic cell carriers. The assembly was coated with 4-15 µm of Parylene C to act as a moisture barrier (additional methods describing Parylene C deposition described below). A clear rectangular polycarbonate window (500 µm thickness, Rowland Technologies Inc.) was epoxied above the four phototransistor detectors to provide a flat optical interface. The boards were coated with 1-3 mm of epoxy (20845, Devcon) for mechanical stability and then casted into PDMS capsules 13mm in diameter (Sylgard 184, Dow Corning).

Parylene C deposition

Electronic components were coated in Parylene-C to provide necessary humidity resilience for the sensitive picoampere-level photocurrent measurements. Di-chloro-di-p-xylylene (brand name: diX C) dimer was purchased from Daisan Kasei Co. (now a KISCO partner company). Thin film Parylene C coating was preformed using an in-house pyrolysis CVD coating tool. After loading the capsules, 10 grams of dimer was loaded into a thermal evaporation heater and the system was evacuated to 1.3 µbar. The pyrolysis furnace and all other vacuum components were pre-heated prior to deposition. During deposition the dimer was evaporated between 105°C to 120°C in order to maintain a constant deposition rate of around 3 Å/s. Upon reaching the desired thickness the deposition chamber was isolated, the system was cooled, the deposition chamber was vented, and the capsules were removed.

Preparation of cell carriers

Cell carriers were machined or injection-molded in ABS plastic (Protolabs Inc.). Semipermeable membranes (0.22 μm pore size, EIMF22205, Millipore Sigma) were affixed to one side of the cell carriers via heat sealing for 35-45 seconds at 230°C with a stainless steel die. Rubber gaskets for fluidic sealing were die-cut from 380 μm silicone rubber (86435K13, McMaster-Carr) and epoxied to the opposite side of the cell carriers to provide a seal between the carrier and the optical window during experiments.

System operation, packet transmission and reception

The NPN phototransistor detectors were operated in a charge-integration mode using each device's intrinsic capacitance as the charge storage mechanism (measured capacitance, C_o = 8.7 nF). The collector of each detector was connected to the supply rail of the system and the emitters were connected to the system ground through independent low-leakage switches (one per detector) in the custom integrated circuit. At the beginning of a measurement, the emitters were shorted to the system ground via the switches and device capacitances were charged to the system voltage. Then, switches were opened and emitter voltages would start to increase independently in response to the dark currents and photo currents in each detector.

The custom integrated circuit contained a low-power voltage reference (V_R = 0.625 V) and local oscillator counter (oscillator period, T_{OSC} = 5 ms). In each oscillator cycle, the detector voltages for each channel were compared to the reference voltage and, if the reference was exceeded, a count value was saved corresponding to the number of oscillator cycles required the charge the channel. The on-board microprocessor polled the custom circuit once every 8 seconds to determine whether all four channels had exceeded

the reference voltage. Once all were exceeded, the microprocessor read the four counter values through a serial peripheral interface and transmitted a short wireless packet at +10 dBm with count data using an on-board transmitter. Two 220 μF ceramic capacitors included in the capsule supplied the instantaneous peak energy required by the radio transmitter. The data were received externally by a 900 MHz wireless radio (CC1120 Evaluation Kit, Texas Instruments Inc.) attached to a laptop and processed offline in Matlab (The Mathworks, Inc.).

Photocurrent estimation with temperature and offset calibration

In each IMBED, one channel acts as a reference to calibrate for background light and temperature-induced dark current variation, while the remaining three are used for independent measurements. The photocurrent detected by the system was estimated from the measured capsule data using an algorithm for temperature drift and offset calibration, which is described as follows:

Let there be three potentially luminescing sensor channels with counts denoted by $N_i: \ i = \{1,2,3\}$. The time required for the photocurrent stimulated by luminescing cells ($I_{PH,i}$) and the dark background current intrinsic to the photodetectors ($I_{D,i}$) to charge the channel capacitance (C_o) of a channel (i) to the threshold voltage (V_R) was quantized using the number of cycles (N_i) counted by the internal oscillator (period, T_{OSC}). The measured cycles were then used to estimate the photocurrent level. The number of cycles required to charge a sensor channel is given by:

$$N_i = \left(\frac{C_o V_R}{T_{OSC}}\right)\left[\frac{1}{I_{D,i} + I_{PH,i}}\right].$$

Let there be one reference channel containing no luminescing cells ($I_{PH} = 0$) with a count denoted by N_r. The number of cycles required to charge the reference is given by:

$$N_r = \left(\frac{C_o V_R}{T_{OSC}}\right)\left[\frac{1}{I_{D,r}}\right].$$

The desired photocurrent signal on a channel ($I_{PH,i}$) is corrupted by the channel's dark current, which we have modelled as:

$$I_{D,r} = I_{D,OS,i} \cdot f(T),$$

by separating a temperature-independent, channel-specific dark current offset ($I_{D,OS,i}$) from a temperature dependent scaling function [$f(T)$].

To calibrate the temperature and offset, the counts from each sensor channel were first compared to the reference channel by calculating a relative signal R_i:

$$R_i = \frac{1/N_i - 1/N_r}{1/N_r} = \left(\frac{I_{D,OS,i} \cdot f(T)}{I_{D,OS,r} \cdot f(T)} - 1\right) + \left[\frac{1}{I_{D,OS,r} \cdot f(T)}\right] I_{PH,i}.$$

In the first term of R_i, the temperature dependence is cancelled, leaving only a dependence on the relative offsets between channels. We can denote this term as $R_{i,OS}$. We used early segments of the count data for each experiment, prior to induction of luminescence from the whole-cell biosensors ($I_{PH,i} = 0$) to estimate $R_{i,OS}$ for each channel. For all experiments, the samples between 0.2 and 0.3 hours (12 to 18 minutes) were used to estimate $R_{i,OS}$. By substituting the measured offset ($R_{i,OS}$), as well as the expression for N_r, we obtained the final expression for the estimated photocurrent in terms of known and measured quantities.

$$I_{PH,i} = \left(\frac{C_O V_R}{T_S N_r}\right)[R_i - R_{i,OS}].$$

This calibration procedure was performed using Matlab software (R2017a, The Mathworks, Inc.).

Optical Calibration

A green LED (λ = 525nm, WP7083ZGD/G, Kingbright) was first calibrated across four decades of input current using an optical power meter located 30 cm away (PM100D and S130C, Thor Labs Inc.). Three capsules were then placed at the same distance as the power meter and measured across the same LED current conditions. The optical power readings were scaled by the ratio of the area of the phototransistor detectors (0.29 mm^2) to the area of the S130C sensor (70.9 mm^2) in order to estimate the optical power incident on the detectors.

Mobile phone "app" for real-time reception and visualization of results

A 900 MHz USB dongle (CC1111 USB Evaluation Module Kit, Texas Instruments, Inc.) was attached to an Android mobile phone (Galaxy SIII, SCH-I535, Samsung Electronics Co. Ltd.) running a custom application created in Android Studio (Google, Inc.). Temperature and offset calibration was performed on the phone after receiving the first 18 minutes of data to enable offset calibration and the photocurrent estimate was displayed to the user. The raw data was simultaneously uploaded to a cloud service for later analysis.

***In vitro* IMBED Experiments**

LB culture media supplemented with or without inducer (500 ppm lysed blood (unless otherwise noted), 10mM thiosulfate, or 100 nM AHL) was pre-warmed for at least 2 hours prior to the start of experiments. For blood sensor experiments, overnight cultures were diluted 1:10 in 2xYTPG (20g tryptone, 5g NaCl, 10g yeast extract, 22 mL

of 1 M potassium phosphate monobasic, 40 mL of 1 M potassium phosphate dibasic, 0.2% glucose, pH 7.2) and 15 µL of diluted culture was added to wells in the cell carrier (approximately 10^6 cells per well). Wild-type *E. coli* Nissle 1917 was added in the reference channel for all experiments. Blood sensor bacteria were added in triplicates to three wells in a single device and values from these three channels were averaged to obtain a single replicate plotted in Figures 2C-E. Technical replicates are depicted in Figure S8. For thiosulfate and AHL experiments, overnight cultures of ThsRS or LuxR containing cells were subcultured for 2 hours in LB prior to addition to cell carriers. Once all four channels were loaded, the cell carrier was fastened to the capsule and fully submerged in pre-warmed media. Cultures were wrapped several times in thick black fabric to block external light, placed in an incubator at 37˚C and data was collected wirelessly for 2 hours. At the end of the experiment, devices were dissembled and cell carriers were discarded. Capsules were sterilized with 70% ethanol and thoroughly washed with distilled water. Capsules were left to air-dry and re-used for future experiments.

Pig Experiments

All pig experiments were approved by the Committee on Animal Care at the Massachusetts Institute of Technology. Female Yorkshire pigs (50-95kg) were obtained from Tufts University and housed under conventional conditions. Animals were randomly selected for the experiments. The animals were placed on a clear liquid diet for 24 hours prior to the experiment with the morning feed held on the day of the experiment. At the time of the experiment, the pigs were sedated with Telazol® (tiletamine/zolazepam 5 mg/kg), xylazine (2 mg/kg) and atropine (0.04 mg/kg). An endoscopic overtube (US

endoscopy) was placed in the esophagus under endoscopic (Pentax) visual guidance during esophageal intubation. Prior to deposition of devices, 250 mL of neutralization solution (1% sodium bicarbonate and 0.2% glucose) with or without 0.25mL of pig blood was administered directly to the stomach through the endoscope. Overnight bacterial cultures were diluted 1:10 in 2xYTPG and 15 µL of diluted culture was added to wells in the cell carriers. Devices were assembled and deposited in the pig gastric cavity via endoscopic overtube. Full submersion in gastric fluid was confirmed by endoscopic observation. For 2 hours, data from deposited capsules was acquired via a 900 MHz radio attached to a laptop or the Android cellular phone. The quality of IMBED sensing was decreased in the pig gastric cavity compared to *in vitro* experiments, potentially due to differences in fluid chemical composition, which could hinder operation of the cells, diffusion rate of heme into the cavities, which could slow the response, and fluid turbidity, which could lower the optical transmission to the photodetectors. Endoscopic videos and radiographs of capsules inside the pig stomach were acquired. Devices were retrieved from the gastric cavity using a hexagonal snare. A total of 6 animals were included in the experiments; 3 were administered neutralization solution containing blood and 3 served as negative controls. Two devices were deposited per pig, such that each group has a sample size of 6.

Note that we observed a small increase in photocurrent in some of the PBS-administered animals, though less than in the heme-administered case. Partial induction of biosensors could be due to low baseline levels of heme present in the gastric cavity of animals in both groups, for example due to dietary heme, scratches of the mucosa during insertion of the endoscope or overtube, or diffusion of heme through the stomach wall.

In addition, small temperature changes caused by the administration of the room temperature neutralization solution (measured to be approximately 5°C) may contribute 2 to 3 pA of effective photocurrent variation as noted in the measurements of Supplemental Fig 7B.

Data Analysis, Statistics and Computational Methods

All data were analyzed using GraphPad Prism version 7.03 (Graph Software, San Diego, CA, USA, http://www.graphpad.com). Sequence analysis was performed using Geneious version 9.1.8 (http://www.geneious.com) (*35*). As noted, error bars represent the SEM of at least three independent experiments carried out on different days. Significance between groups was determined using an unpaired, two-tailed Student's t-test assuming unequal variance. Fold change or signal-to-noise ratio was determined by dividing the normalized luminescence values (RLU/CFU) of samples treated with the maximal inducer concentration with uninduced samples. Response curves were fit to a Hill function: $Y=(B_{max}X^n)/(K^n+X^n) + C$, where X is the inducer concentration, Y is the normalized luminescence output, B_{max} is the maximum luminescence, K is the threshold constant, n is the Hill coefficient and C is the baseline luminescence.

Supplementary Figures

Fig. S1

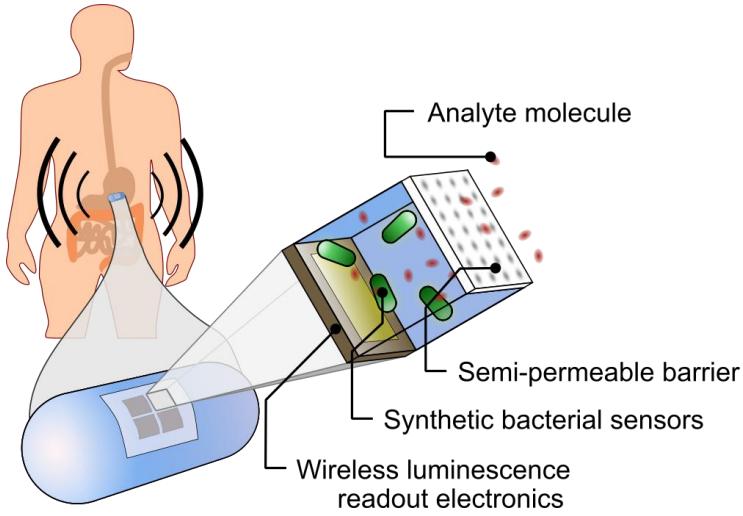

Figure S1. Capsule for sensing biomarkers *in vivo* with whole-cell bacterial sensors and wireless electronic readout.

Fig. S2

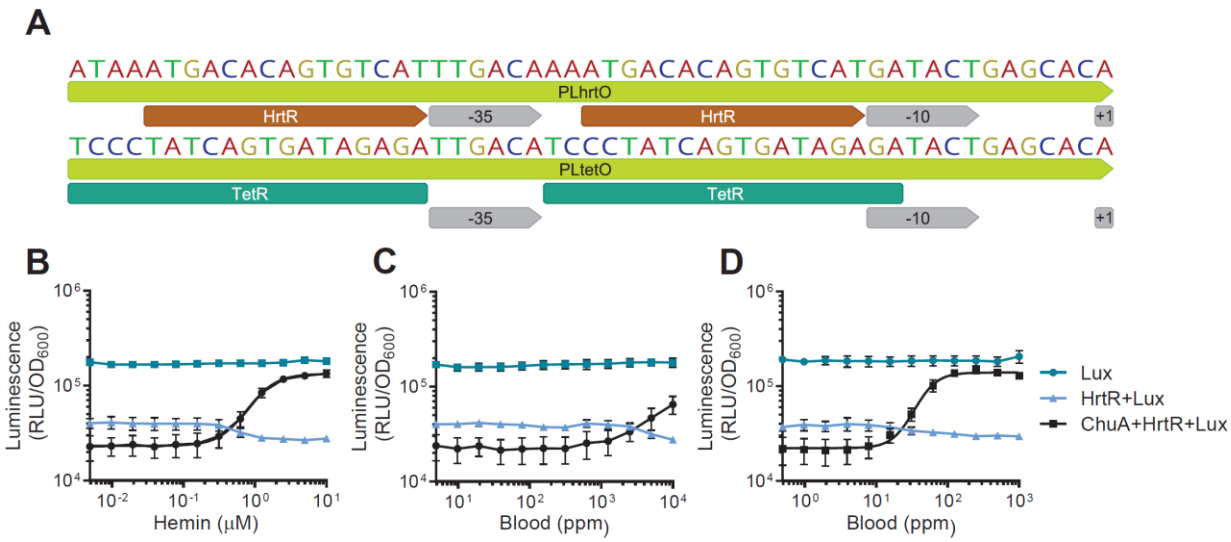

Figure S2. Design and *in vitro* evaluation of prototype heme sensing genetic circuit.

(A) Promoter design of heme-responsive promoter. The TetR operator sites of a synthetic promoter based on the left promoter of bacteriophage lambda ($P_{L(TetO)}$) (cite Lutz and Bujard) were replaced with the operator DNA sequences to which HrtR binds. Spacing between the -10 and -35 sites was preserved. (B-D) Dose-response curves of prototype genetic circuits in *E. coli* MG1655 in various concentrations of hemin (B), whole horse blood (C), and blood lysed in simulated gastric fluid (D). The genetic circuit contains $P_{L(HrtO)}$-*luxCDABE* alone (Lux), $P_{L(HrtO)}$-*luxCDABE* with the HrtR transcriptional repressor (HrtR+Lux), or $P_{L(HrtO)}$-*luxCDABE*, HrtR and the ChuA heme transporter (ChuA+HrtR+Lux). Luminescence values are measured 2 hours post-exposure to inducer and normalized to the optical density of the culture. Error bars represent SEM of three independent biological replicates.

Fig. S3

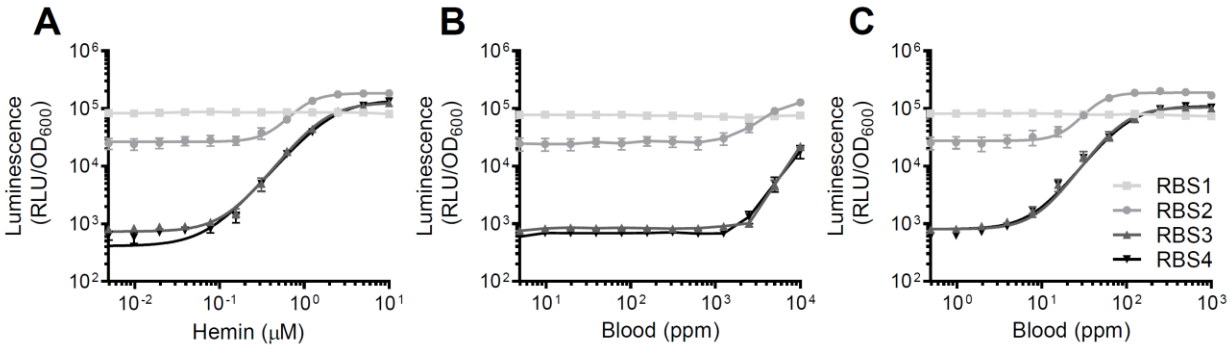

D

RBS	Predicted Strength (AU)
1	1783.6
2	3877.1
3	33545.5
4	599195.9

Figure S3. Genetic circuit optimization by varying translational initiation strength of HrtR. Dose-response curves of heme-sensing genetic circuits in *E. coli* MG1655 in various concentrations of hemin (A), whole horse blood (B), and blood lysed in simulated gastric fluid (C). The translational initiation strength of HrtR was varied using different computationally-designed ribosome binding sites (RBS) (cite Salis and Esbah). Predicted RBS strengths are listed in D. Luminescence values are measured 2 hours post-exposure to inducer and normalized to the optical density of the culture. Error bars represent SEM of three independent biological replicates. In addition to varying HrtR RBS strength, genetic components were combined onto a single high copy plasmid to minimize plasmid burden as well as the risk of plasmid loss. Variations in promoter sequence, number and position of HrtO operator sites in $P_{L(HrtO)}$, were explored as a means to alter the affinity of HrtR to $P_{L(HrtO)}$. However, these strategies did not appreciably change the heme induction response. Similarly, modifications to ChuA RBS strength to control the heme-import bottleneck did not lead to appreciable improvements in gene circuit performance.

Fig. S4

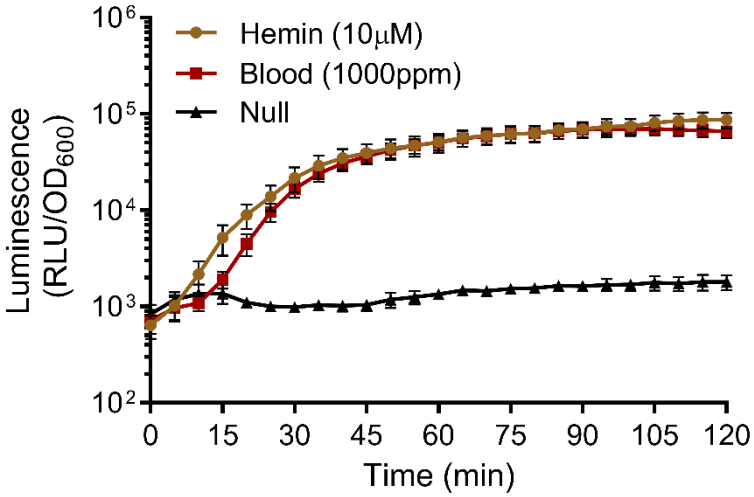

Figure S4. Kinetic response of blood biosensor strain. *E. coli* Nissle blood biosensors (Nissle V2 from Figure 1B) were treated with 10 μM hemin (brown), 1000 ppm blood (red) or PBS (black) and luminescence response was measured in a plate reader every 5 minutes for 2 hours. Luminescence values are normalized to the optical density of the bacterial culture. Error bars represent SEM of three independent biological experiments.

Fig. S5

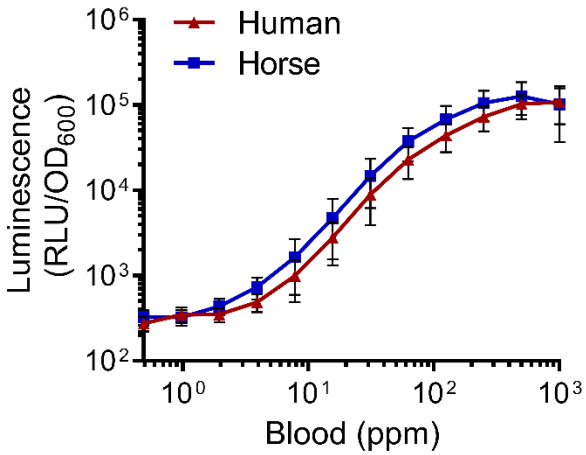

Figure S5. Blood biosensors responds to blood of different mammalian origins. *E. coli* Nissle blood sensor strains (Nissle V2 from Figure 1B) were treated with various concentrations of human or horse blood lysed in simulated gastric fluid. Luminescence values are measured 2 hours post-exposure to inducer and normalized to the optical density of the culture. Error bars represent SEM of three independent biological replicates.

Fig. S6

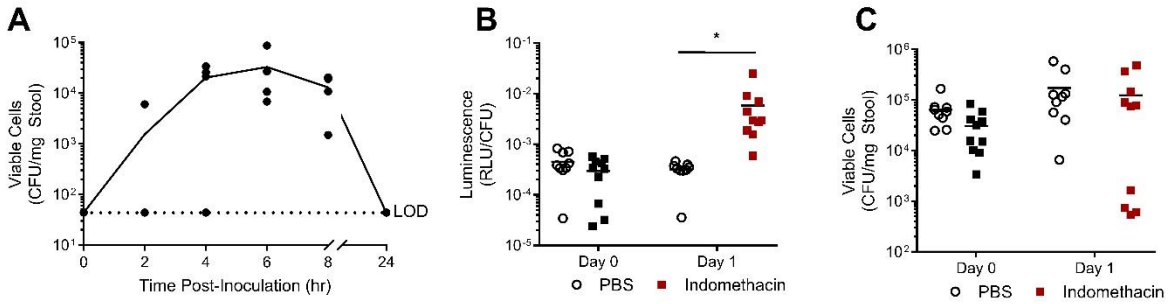

Figure S6. Heme biosensors can detect blood in an *in vivo* murine model of indomethacin-induced gastrointestinal bleeding. (A) C57BL/6J mice were inoculated with approximately $2x10^8$ CFU of blood biosensors by oral gavage (n=4). Fecal pellets were collected from mice prior to gavage and at 2, 4, 6, 8 and 24 hours post-gavage and plated to determine CFU counts. All mice contained biosensor bacteria in their stool 6 hours post-gavage and no colonization was observed. Dotted line indicates the limit of detection (LOD) of the assay. (B) Mice were inoculated with approximately $2x10^8$ CFU of *E. coli* Nissle blood sensors 6 hours prior to (Day 0) or 16 hours after (Day 1) administration of indomethacin (10 mg/kg) or PBS buffer as a negative control. Induction of bleeding was confirmed by guaiac test (indicated by red color). Fecal pellets were collected from animals 6 hours post-gavage, homogenized and analyzed for luminescence production as well as plated to enumerate colony forming units (CFU). Luminescence values were normalized to cell number in fecal pellets (N = 10). *P<0.05, Student's t-test. (C) CFU counts in fecal pellets 6 hours post-gavage.

Fig. S7

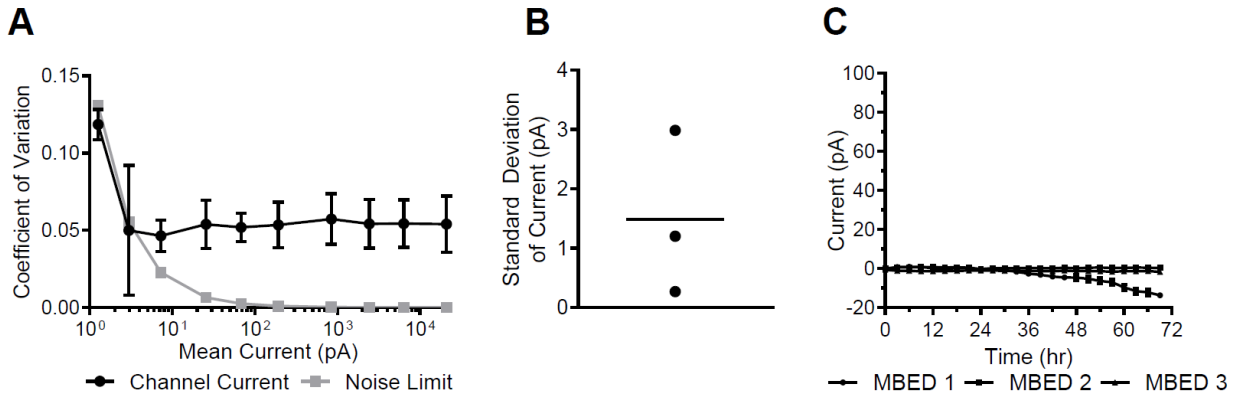

Figure S7. Capsule readout variation was characterized across optical input power, temperature change and fluid submersion. (A) The coefficient of variation between measurements on three channels within a single device, characterized across input light intensity (N = 3 devices). At low signal levels, the measurement standard deviation is limited by white noise (13%$_{rms}$ noise at 1.3pA). At higher signal levels, it is limited by mismatch between the channels (< 6%$_{rms}$ above 3pA). (B) Residual variation induced by temperature change, post-calibration. The temperature was stepped from 35°C to 40°C (temperature change 5°C) and the standard deviation across three sensor channels was measured (N = 3 devices). (C) Stability of the measurements from IMBED devices in Simulated Gastric Fluid (SGF) for 72 hours (N = 3). For two devices, current values were stable for the duration of measurement. The third system operated for 36 hours before corruption by humidity became evident.

Fig. S8

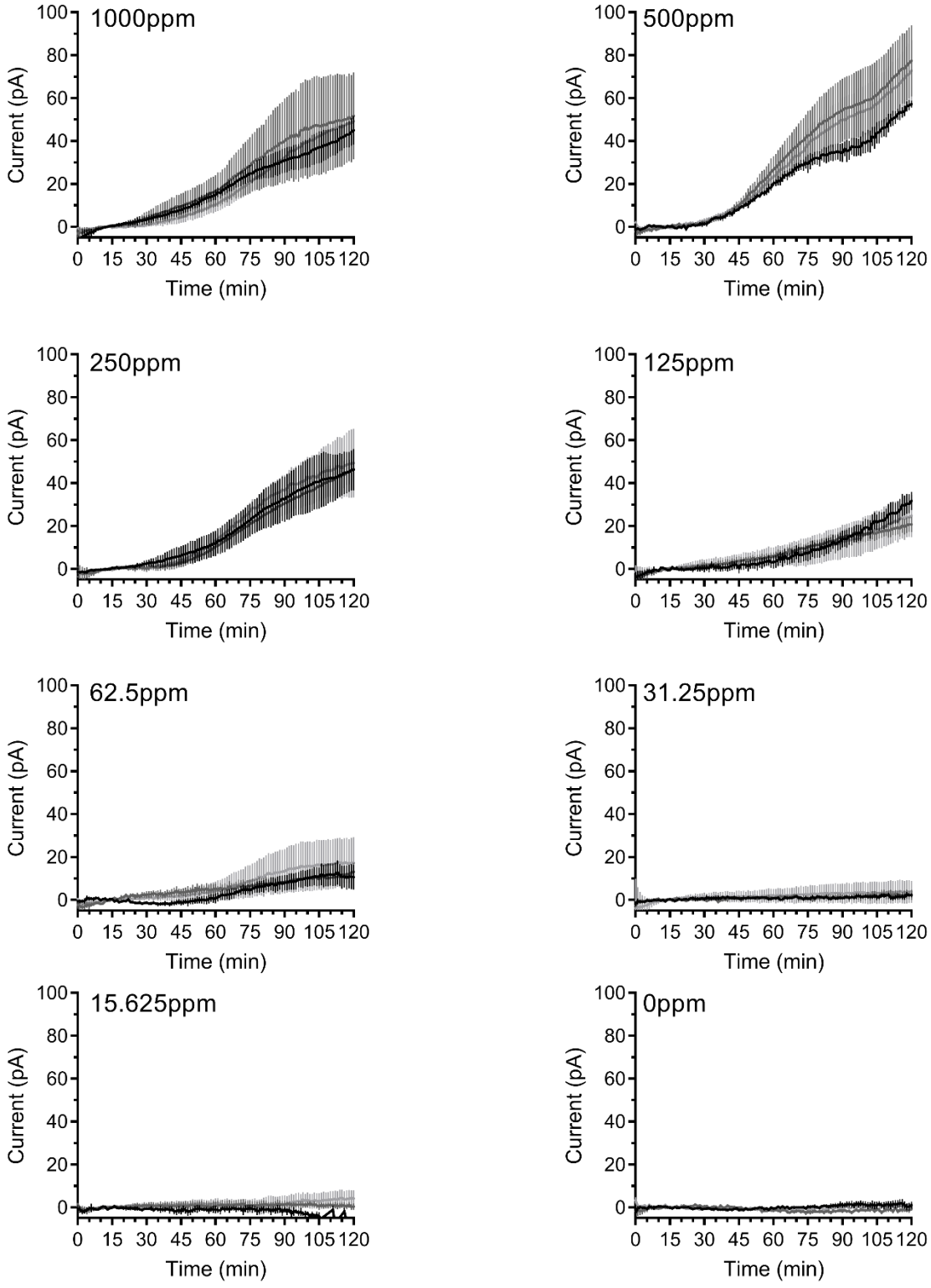
1000ppm
500ppm
250ppm
125ppm
62.5ppm
31.25ppm
15.625ppm
0ppm
Current (pA)
Time (min)
0 15 30 45 60 75 90 105 120
0 20 40 60 80 100

Figure S8. Technical replicates of blood sensor IMBED across various blood concentrations. Overnight cultures of *E. coli* Nissle blood biosensors were diluted in fresh 2xYTPG and loaded in an IMBED in triplicates. Wild-type Nissle was loaded in the reference channel. The assembled device was submerged in pre-warmed LB supplemented with the indicated concentration of blood. Each line depicts a biological replicate of the mean response of a single IMBED for a given concentration of blood. Compared to plate-reader experiments (fig. S5), there is a slightly time delay in luminescence response for IMBEDs submerged in fluid containing blood. This difference likely owes to the diffusion time of heme into the cell cavities. Error bars represent the standard deviation of the three replicate channels within a single device.

Fig. S9

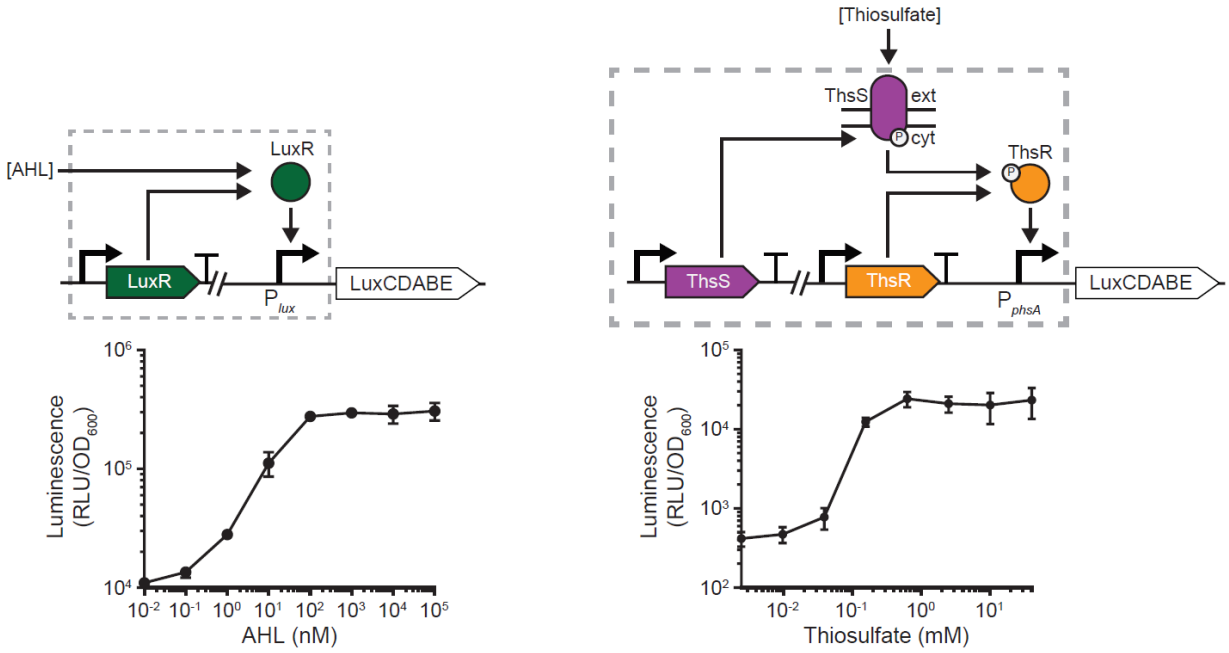

Figure S9. Design and characterization of acyl-homoserine lactone (AHL) and thiosulfate-responsive biosensors. AHL binds to the transcriptional activator LuxR that activates transcription of the *luxCDABE* operon downstream of the P_{lux} promoter. Titrating increasing amounts of AHL yields high levels of luminescence. The ThsRS two-component system mediated thiosulfate-inducible expression of the *luxCDABE* operon from the P_{phsA} promoter. Thiosulfate binds to the membrane bound ThsS histidine kinase that, in turn, phosphorylates the ThsR response regulator such that it can activate transcription from P_{phsA}. Error bars indicate SEM from three independent biological replicates.

Fig. S10

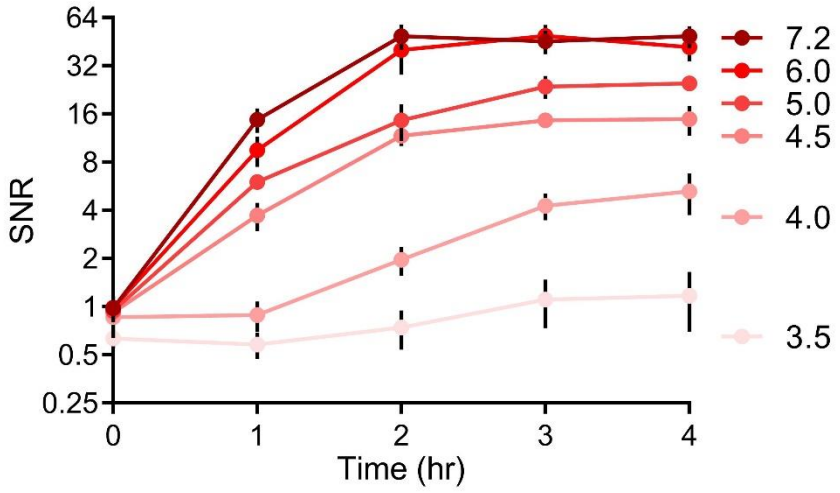

Figure S10. Kinetic response of blood biosensor strains at various pHs. *E. coli* Nissle blood biosensors (Nissle V2 from Figure 1B) were treated with 500 ppm blood or PBS in citrate-buffered LB at various pHs. Luminescence response was measured in a plate reader every hour for 4 hours. The signal-to-noise ratio (SNR) of each sample at each timepoint was calculated by dividing the OD_{600}-normalized luminescence values of induced by the OD_{600}-normalized luminescence values of uninduced samples. The integrity of the genetic circuit degrades with decreasing pH and is non-functional below pH4.0. Error bars represent SEM of three independent biological experiments.

Fig. S11

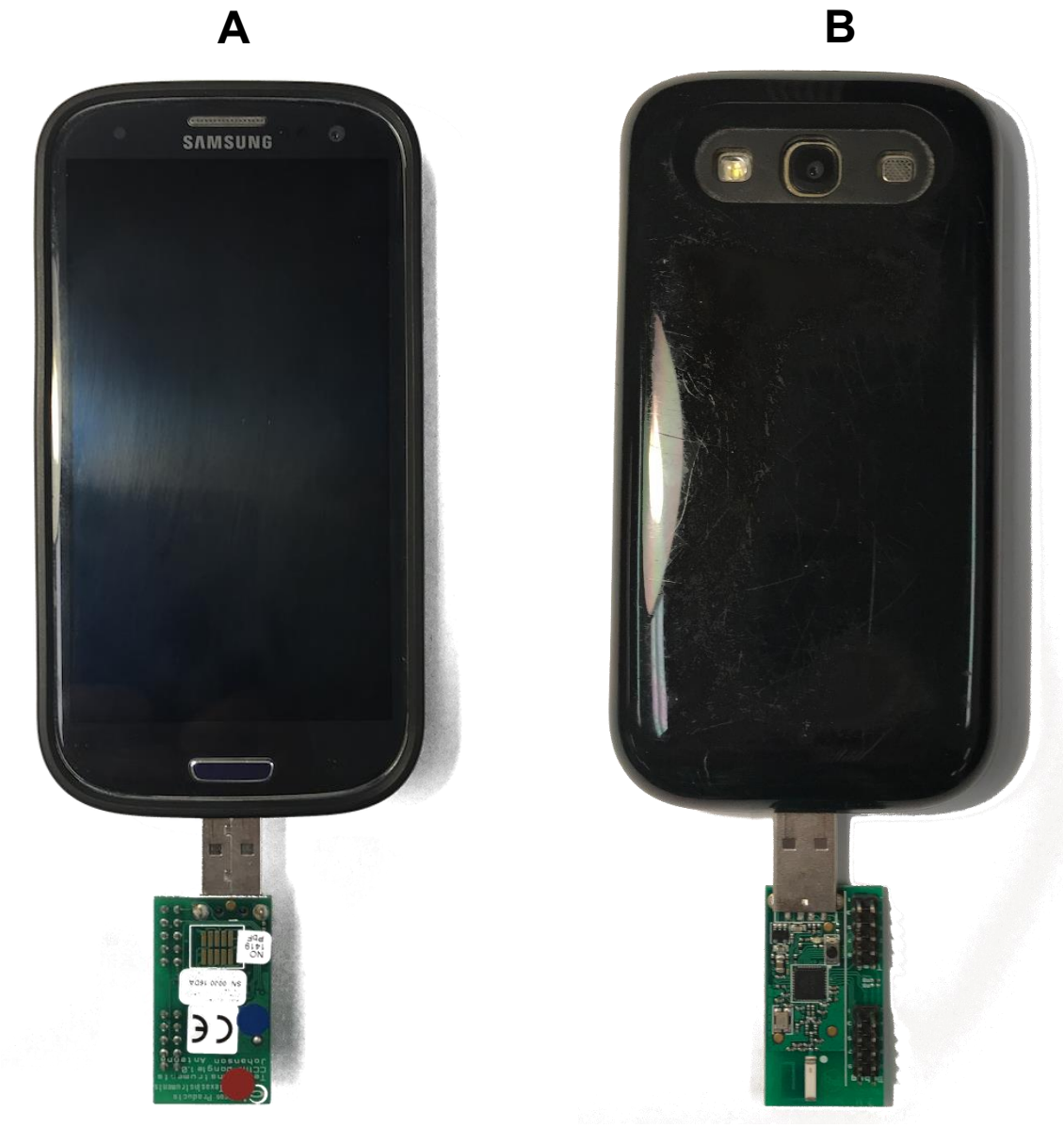

Figure S11. Mobile phone and 900 MHz wireless receiver dongle used for visualizing IMBED measurement results and logging them to the cloud. The receiver dongle connects to the phone via USB and delivers packets received wirelessly from the IMBED device to application software. The software uploads data to a cloud service and performs visualization for the user.

Fig. S12

Figure S12. Application software displaying IMBED measurement results to the user on a mobile phone. Representative data received from the IMBED device during a porcine study with administration of (A) the buffer solution, and (B) the blood solution.

Fig. S13

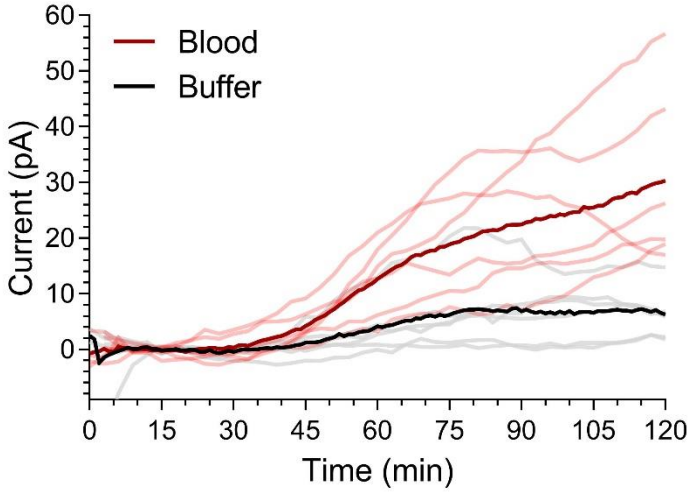

Figure S13. Individual replicates of blood sensing IMBEDs in the pig gastric environment. Blood sensor IMBEDs were deposited in the gastric cavity of pigs administered neutralization solution containing 0.25mL of blood (red) or buffer alone (black). Readings from IMBEDs were wirelessly collected for 120 minutes following device deposition. Dark trace represent the mean of 6 replicate IMBEDs (3 animals on different days, 2 devices per pig) and pale traces indicate the individual current values for a given IMBED.

Fig. S14

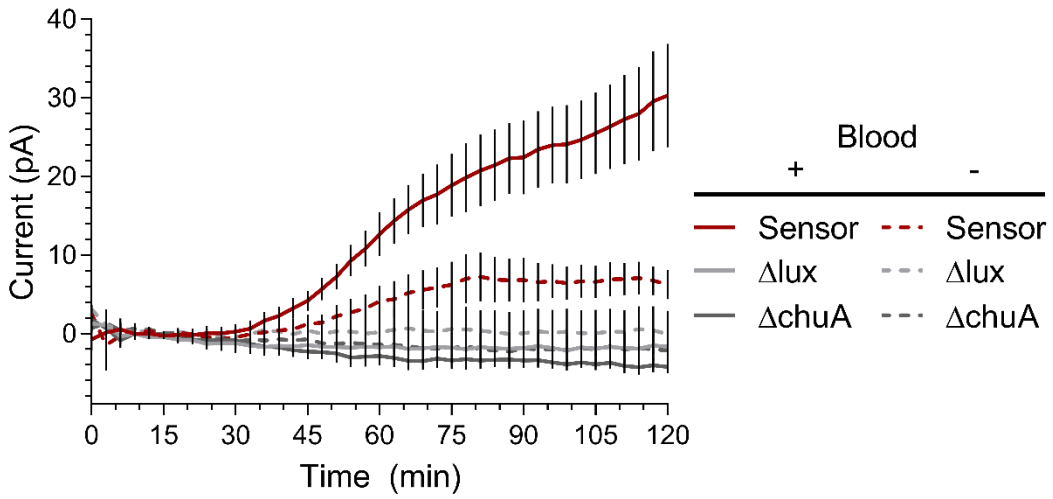

Figure S14. Functional blood biosensing genetic circuits are necessary for IMBED detection of blood in the pig gastric environment. *E. coli* Nissle strains containing a functional biosensor circuit (Sensor), a circuit lacking the luciferase output (Δlux), and a circuit lacking the heme transporter ChuA (ΔchuA) were loaded into a IMBED. Devices were deposited in the stomach of animals administered neutralization solution spiked with blood or with buffer alone. IMBED readings were wirelessly collected for 120 minutes post-device deposition. Only channels that correspond to functional biosensors in pigs administered blood display high levels of luminescence. Endogenous levels of heme in the pig stomach as well as the cellular response to the pig gastric environment are not sufficient to generate high levels of bioluminescence. Error bars denote SEM for six IMBED experiments (3 animals on different days, 2 capsules per animal).

Table S1

Current consumption		
System (excluding wireless)		
System leakage		0.30 μA
Microcontroller		0.42 μA
ULP Luminescence Chip		0.01 μA
Wireless		
Active wireless current	16.5 mA	
Packet bits	296 bits	
Bit rate	50 kbps	
Packet time	5.92 ms	
Sampling interval	25 s	
Duty cycle	2.4×10^{-4}	
Average wireless current		3.96 μA
Total average current		4.69 μA
Total average power (@ 2.7V)		12.7 μW

Table S1. Average current consumption of the capsule system. The System Leakage is the static current consumed with all functions of the capsule disabled. The commercial Microcontroller average consumption arises from polling of the luminescence chip every 8 seconds to determine whether a measurement has been completed. The ULP Luminescence Chip consumption results from the continuous operation of the luminescence quantification circuitry. The Wireless consumption results from the transmission of packets. The commercial wireless transmitter dominates the total system consumption (84.4%), whereas the custom illuminometer consumes only a small fraction of the total (< 0.2%). The small button-cell battery (5 mAh) inside the capsule could power the device for up to 1.5 months on a full charge, or up to 9 months in sleep mode with the wireless disabled.

Additional Data Table S2 (separate file)

Genetic Parts: Description and sequence of genetic parts used in this study.

Additional Data Table S3 (separate file)

Plasmids: Description of plasmids used in this study.

References and Notes

1. J. A. N. Brophy, C. A. Voigt, Principles of genetic circuit design. *Nat. Methods* **11**, 508–520 (2014). doi:10.1038/nmeth.2926 Medline

2. S. Slomovic, K. Pardee, J. J. Collins, Synthetic biology devices for in vitro and in vivo diagnostics. *Proc. Natl. Acad. Sci. U.S.A.* **112**, 14429–14435 (2015). doi:10.1073/pnas.1508521112 Medline

3. C. Roggo, J. R. van der Meer, Miniaturized and integrated whole cell living bacterial sensors in field applicable autonomous devices. *Curr. Opin. Biotechnol.* **45**, 24–33 (2017). doi:10.1016/j.copbio.2016.11.023 Medline

4. A. Courbet, D. Endy, E. Renard, F. Molina, J. Bonnet, Detection of pathological biomarkers in human clinical samples via amplifying genetic switches and logic gates. *Sci. Transl. Med.* **7**, 289ra83 (2015). doi:10.1126/scitranslmed.aaa3601 Medline

5. J. W. Kotula, S. J. Kerns, L. A. Shaket, L. Siraj, J. J. Collins, J. C. Way, P. A. Silver, Programmable bacteria detect and record an environmental signal in the mammalian gut. *Proc. Natl. Acad. Sci. U.S.A.* **111**, 4838–4843 (2014). doi:10.1073/pnas.1321321111 Medline

6. M. Mimee, A. C. Tucker, C. A. Voigt, T. K. Lu, Programming a human commensal bacterium, *Bacteroides thetaiotaomicron*, to sense and respond to stimuli in the murine gut microbiota. *Cell Syst.* **1**, 62–71 (2015). Medline

7. B. Lim, M. Zimmermann, N. A. Barry, A. L. Goodman, Engineered regulatory systems modulate gene expression of human commensals in the gut, engineered regulatory systems modulate gene expression of human commensals in the gut. *Cell* **169**, 547–558.e15 (2017). doi:10.1016/j.cell.2017.03.045 Medline

8. K. N.-M. Daeffler, J. D. Galley, R. U. Sheth, L. C. Ortiz-Velez, C. O. Bibb, N. F. Shroyer, R. A. Britton, J. J. Tabor, Engineering bacterial thiosulfate and tetrathionate sensors for detecting gut inflammation. *Mol. Syst. Biol.* **13**, 923 (2017). doi:10.15252/msb.20167416 Medline

9. D. T. Riglar, T. W. Giessen, M. Baym, S. J. Kerns, M. J. Niederhuber, R. T. Bronson, J. W. Kotula, G. K. Gerber, J. C. Way, P. A. Silver, Engineered bacteria can function in the mammalian gut long-term as live diagnostics of inflammation. *Nat. Biotechnol.* **35**, 653–658 (2017). doi:10.1038/nbt.3879 Medline

10. J. M. Pickard, C. F. Maurice, M. A. Kinnebrew, M. C. Abt, D. Schenten, T. V. Golovkina, S. R. Bogatyrev, R. F. Ismagilov, E. G. Pamer, P. J. Turnbaugh, A. V. Chervonsky, Rapid fucosylation of intestinal epithelium sustains host-commensal symbiosis in sickness. *Nature* **514**, 638–641 (2014). doi:10.1038/nature13823 Medline

11. B. Otis, B. Parviz, Introducing our smart contact lens project. *Google Off. Blog* (2014); https://googleblog.blogspot.com/2014/01/introducing-our-smart-contact-lens.html.

12. H. Wang, Magnetic sensors for diagnostic medicine: CMOS-based magnetic particle detectors for medical diagnosis applications. *IEEE Microw. Mag.* **14**, 110–130 (2013). doi:10.1109/MMM.2013.2259402

13. H. Norian, R. M. Field, I. Kymissis, K. L. Shepard, An integrated CMOS quantitative-polymerase-chain-reaction lab-on-chip for point-of-care diagnostics. *Lab Chip* **14**, 4076–4084 (2014). doi:10.1039/C4LC00443D Medline

14. G. Iddan, G. Meron, A. Glukhovsky, P. Swain, Wireless capsule endoscopy. *Nature* **405**, 417–417 (2000). doi:10.1038/35013140 Medline

15. K. Kalantar-Zadeh *et al.*, A human pilot trial of ingestible electronic capsules capable of sensing different gases in the gut. *Nat. Electron. 2017 11*. **1**, 79 (2018).

16. P. J. van der Schaar, J. F. Dijksman, H. Broekhuizen-de Gast, J. Shimizu, N. van Lelyveld, H. Zou, V. Iordanov, C. Wanke, P. D. Siersema, A novel ingestible electronic drug delivery and monitoring device. *Gastrointest. Endosc.* **78**, 520–528 (2013). doi:10.1016/j.gie.2013.03.170 Medline

17. H. Hafezi, T. L. Robertson, G. D. Moon, K.-Y. Au-Yeung, M. J. Zdeblick, G. M. Savage, An ingestible sensor for measuring medication adherence. *IEEE Trans. Biomed. Eng.* **62**, 99–109 (2015). doi:10.1109/TBME.2014.2341272 Medline

18. P. Nadeau, M. Mimee, S. Carim, T. K. Lu, A. P. Chandrakasan, Nanowatt circuit interface to whole-cell bacterial sensors. *2017 IEEE International Solid-State Circuits Conference (ISSCC)*, San Francisco, CA, 2017, pp. 352–353.

19. D. C. Rockey, J. Koch, J. P. Cello, L. L. Sanders, K. McQuaid, Relative frequency of upper gastrointestinal and colonic lesions in patients with positive fecal occult-blood tests. *N. Engl. J. Med.* **339**, 153–159 (1998). doi:10.1056/NEJM199807163390303 Medline

20. A. Barkun, M. Bardou, J. K. Marshall; Nonvariceal Upper GI Bleeding Consensus Conference Group, Consensus recommendations for managing patients with nonvariceal upper gastrointestinal bleeding. *Ann. Intern. Med.* **139**, 843–857 (2003). doi:10.7326/0003-4819-139-10-200311180-00012 Medline

21. D. Lechardeur, B. Cesselin, U. Liebl, M. H. Vos, A. Fernandez, C. Brun, A. Gruss, P. Gaudu, Discovery of intracellular heme-binding protein HrtR, which controls heme efflux by the conserved HrtB-HrtA transporter in *Lactococcus lactis*. *J. Biol. Chem.* **287**, 4752–4758 (2012). doi:10.1074/jbc.M111.297531 Medline

22. C. L. Nobles, J. R. Clark, S. I. Green, A. W. Maresso, A dual component heme biosensor that integrates heme transport and synthesis in bacteria. *J. Microbiol. Methods* **118**, 7–17 (2015). doi:10.1016/j.mimet.2015.07.011 Medline

23. D. Close, T. Xu, A. Smartt, A. Rogers, R. Crossley, S. Price, S. Ripp, G. Sayler, The evolution of the bacterial luciferase gene cassette (*lux*) as a real-time bioreporter. *Sensors (Basel)* **12**, 732–752 (2012). doi:10.3390/s120100732 Medline

24. A. Lanas, F. K. L. Chan, Peptic ulcer disease. *Lancet* **390**, 613–624 (2017). doi:10.1016/S0140-6736(16)32404-7 Medline

25. H. Eltoukhy, K. Salama, A. El Gamal, A 0.18-µm CMOS bioluminescence detection lab-on-chip. *IEEE J. Solid-State Circuits* **41**, 651–662 (2006). doi:10.1109/JSSC.2006.869785

26. R. R. Singh, L. Leng, A. Guenther, R. Genov, A CMOS-microfluidic chemiluminescence contact imaging microsystem. *IEEE J. Solid-State Circuits* **47**, 2822–2833 (2012). doi:10.1109/JSSC.2012.2214182

27. I. Y. Hwang, E. Koh, A. Wong, J. C. March, W. E. Bentley, Y. S. Lee, M. W. Chang, Engineered probiotic *Escherichia coli* can eliminate and prevent *Pseudomonas aeruginosa* gut infection in animal models. *Nat. Commun.* **8**, 15028 (2017). doi:10.1038/ncomms15028 Medline

28. M. Schuster, D. J. Sexton, S. P. Diggle, E. P. Greenberg, Acyl-homoserine lactone quorum sensing: From evolution to application. *Annu. Rev. Microbiol.* **67**, 43–63 (2013). doi:10.1146/annurev-micro-092412-155635 Medline

29. A. M. Bellinger, M. Jafari, T. M. Grant, S. Zhang, H. C. Slater, E. A. Wenger, S. Mo, Y. L. Lee, H. Mazdiyasni, L. Kogan, R. Barman, C. Cleveland, L. Booth, T. Bensel, D. Minahan, H. M. Hurowitz, T. Tai, J. Daily, B. Nikolic, L. Wood, P. A. Eckhoff, R. Langer, G. Traverso, Oral, ultra-long-lasting drug delivery: Application toward malaria elimination goals. *Sci. Transl. Med.* **8**, 365ra157 (2016). doi:10.1126/scitranslmed.aag2374 Medline

30. A. R. Kirtane, O. Abouzid, D. Minahan, T. Bensel, A. L. Hill, C. Selinger, A. Bershteyn, M. Craig, S. S. Mo, H. Mazdiyasni, C. Cleveland, J. Rogner, Y. L. Lee, L. Booth, F. Javid, S. J. Wu, T. Grant, A. M. Bellinger, B. Nikolic, A. Hayward, L. Wood, P. A. Eckhoff, M. A. Nowak, R. Langer, G. Traverso, Development of an oral once-weekly drug delivery system for HIV antiretroviral therapy. *Nat. Commun.* **9**, 2 (2018). doi:10.1038/s41467-017-02294-6 Medline

31. D. G. Gibson, L. Young, R.-Y. Chuang, J. C. Venter, C. A. Hutchison 3rd, H. O. Smith, Enzymatic assembly of DNA molecules up to several hundred kilobases. *Nat. Methods* **6**, 343–345 (2009). doi:10.1038/nmeth.1318 Medline

32. C. T. Chung, S. L. Niemela, R. H. Miller, One-step preparation of competent *Escherichia coli*: Transformation and storage of bacterial cells in the same solution. *Proc. Natl. Acad. Sci. U.S.A.* **86**, 2172–2175 (1989). doi:10.1073/pnas.86.7.2172 Medline

33. H. M. Salis, E. A. Mirsky, C. A. Voigt, Automated design of synthetic ribosome binding sites to control protein expression. *Nat. Biotechnol.* **27**, 946–950 (2009). doi:10.1038/nbt.1568 Medline

34. A. Espah Borujeni, A. S. Channarasappa, H. M. Salis, Translation rate is controlled by coupled trade-offs between site accessibility, selective RNA unfolding and sliding at upstream standby sites. *Nucleic Acids Res.* **42**, 2646–2659 (2014). doi:10.1093/nar/gkt1139 Medline

35. M. Kearse, R. Moir, A. Wilson, S. Stones-Havas, M. Cheung, S. Sturrock, S. Buxton, A. Cooper, S. Markowitz, C. Duran, T. Thierer, B. Ashton, P. Meintjes, A. Drummond, Geneious Basic: An integrated and extendable desktop software platform for the organization and analysis of sequence data. *Bioinformatics* **28**, 1647–1649 (2012). doi:10.1093/bioinformatics/bts199 Medline